

Fabrication and Compression Properties of Functionally Graded Copper Foam Made Using Friction Powder Sintering and Dissolution

Yoshihiko Hangai, Kousuke Zushida, Hidetoshi Fujii, Osamu Kuwazuru, and Nobuhiro Yoshikawa

(Submitted August 2, 2016; in revised form July 20, 2017; published online September 6, 2017)

Functionally graded (FG) metal foams have properties that vary with the position, giving them controlled compression deformation behavior with the desired plateau stresses. In this contribution, bilayer FG Cu foams consisting of a high-porosity layer and a low-porosity layer were fabricated and their compression properties were demonstrated. A friction powder sintering process based on the sintering and dissolution process was employed to fabricate the FG Cu foams. X-ray computed tomography observations revealed that the porosity markedly changed around the boundary between the layers of the FG Cu foam with NaCl volume fractions of $V_f = 80\%$ (high porosity) and $V_f = 60\%$ (low porosity), and the two layers exhibited almost constant porosities and were bonded seamlessly. From compression tests on the fabricated FG Cu foams, it was found that the $V_f = 80\%$ layer first deformed while the $V_f = 60\%$ layer hardly deformed at the beginning of the compression. Thereafter, the $V_f = 60\%$ layer started to deform. From the compression stress–strain curves, the FG Cu foams exhibited two plateau regions with low and high plateau stresses corresponding to the deformation behavior. The first plateau stress and second plateau stress obtained from the FG Cu foams exhibited similar values to those obtained from uniform Cu foams with $V_f = 80\%$ and $V_f = 60\%$, respectively. Moreover, Cu foams consisting of simply stacked uniform Cu foams with $V_f = 80\%$ and $V_f = 60\%$ without bonding exhibited almost the same deformation behavior and compression properties except for slightly larger dispersion than that in the FG Cu foams, which is considered to be due to the lack of bonding and the discontinuity between the pores at the boundary between the $V_f = 80\%$ and $V_f = 60\%$ layers.

Keywords cellular materials, functionally gradient materials, powder metallurgy, sintering

1. Introduction

Functionally graded (FG) metal foams have properties that vary with the position and are expected to be lightweight and possess superior properties to ordinary metallic foams. Several processing routes for fabricating FG metallic foams have been proposed, such as the casting space holder process (Ref 1, 2), the powder metallurgy space holder process (Ref 3), the precursor foaming process (Ref 4–10) and the metal melt direct foaming process (Ref 11). In these processes, the properties variation is adjusted via the position-dependent pore structures (pore size, pore morphology and porosity) (Ref 1–8, 11) and the alloy composition (Ref 9, 10). It is expected that FG metallic foams will have controlled compression deformation behavior with the desired plateau stresses corresponding to the compression properties of the metallic foams by controlling the pore structure and alloy

composition at each position (Ref 6–10). However, accurate control of the pore structure at the desired position is relatively difficult; therefore, there have been few investigations on the properties of FG metallic foams as structural materials. In addition, these studies mainly focused on aluminum (Al) foam owing to the difficulty of fabricating foams of high-melting-point metals. It is expected that the realization of FG metallic foams other than those of Al will expand the use of metallic foams in various industrial fields. In particular, copper (Cu) foam can be used as an engineering material when efficient heat exchange is required (Ref 12, 13). Also, Cu foam is expected to exhibit superior compression properties to Al foam. Therefore, FG Cu foam with the desired pore structure at each position is expected to have a greatly improved performance as an engineering material.

To realize the accurate control of pore structures, a sintering and dissolution process (SDP) has been proposed by Zhao and Sun for the fabrication of Al foam (Ref 14). In the SDP process, Al powder and sodium chloride (NaCl) powder as space holders are mixed and sintered. Then, the NaCl in the mixture is dissolved by immersing the mixture in water, resulting in an Al foam. The SDP process has several advantages for fabricating Al foam. First, by controlling the volume fraction and particle shape of the NaCl powder, the pore structures of the Al foam are easily controlled. Second, NaCl is easily removed from the sintered mixture by simply immersing the mixture in water. Third, NaCl retains its initial shape without deforming or melting during the sintering process because its melting point (1074 K) is higher than that of Al (933 K). Fourth, NaCl is inexpensive, readily available, nontoxic and rapidly dissolves in water.

Yoshihiko Hangai and Kousuke Zushida, Graduate School of Science and Technology, Gunma University, Kiryu 376-8515, Japan; Hidetoshi Fujii, Joining and Welding Research Institute, Osaka University, Ibaraki 567-0047, Japan; Osamu Kuwazuru, Graduate School of Engineering, University of Fukui, Fukui 910-8507, Japan; and Nobuhiro Yoshikawa, Institute of Industrial Science, The University of Tokyo, Tokyo 153-8505, Japan. Contact e-mail: hanhan@gunma-u.ac.jp.

A friction powder sintering (FPS) process based on the SDP has been proposed for the fabrication of metallic foams (Ref 15-17). In the FPS process, a mixture of a metal and NaCl powder is sintered by the friction heat and pressing pressure generated by plunging a rotating tool into a metal plate die with the mixture filling a hole in the die. The FPS process is easy to conduct and has low environmental impact because an external heat source is not necessary, except for the friction heat generated in the vicinity of the mixture. Furthermore, only a conventional milling machine is necessary, i.e., no special equipment is required, enabling metallic foam to be manufactured at a low cost.

In a previous study (Ref 17), Cu foams with NaCl volume fractions V_f in the mixture of 60, 70 and 80% were fabricated by the FPS process. Although the melting point of Cu (1356 K) is much higher than that of NaCl (1074 K), it was shown that no further sintering of the Cu matrix was necessary during or after the dissolution of NaCl, which is essential in other processes using space holders (Ref 18-20), because it was found that a lower temperature than the melting point of NaCl can be employed during the FPS process. Ductile deformation behavior was observed during the compression tests on the obtained Cu foams regardless of their porosity, indicating that the sintering of the Cu particles was achieved by the FPS process. The plateau stress decreased as the porosity increased with a strong correlation between them. Namely, it is expected that by varying V_f , the mechanical properties of Cu foams can be easily controlled.

In this study, bilayer FG Cu foams with $V_f = 60$ and 80% were fabricated by the FPS process. Scanning electron microscopy (SEM) and x-ray computed tomography (x-ray CT) inspections were conducted on the FG Cu foams to confirm that different porosities (volume fractions of pores) were achieved in the two layers and that the pore shape was similar to that of the NaCl particles. Furthermore, the Cu foams were subjected to compression tests to observe their deformation behavior in comparison with those of uniform Cu foams with $V_f = 60$ and 80%. Moreover, uniform Cu foams with $V_f = 60$ and 80% were simply stacked similarly to that in the FG Cu foam except without bonding, and the compression properties were compared with those of the FG Cu foam.

2. Experimental Procedure

2.1 FPS Process

Figure 1 shows a schematic illustration of the FPS process for fabricating FG Cu foam. First, Cu and NaCl powders with

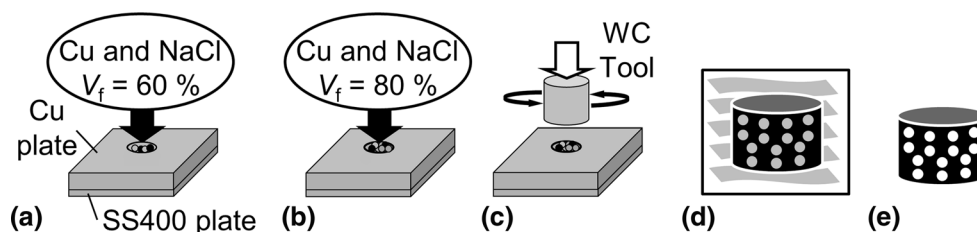


Fig. 1 Schematic of FPS process for fabricating FG Cu foam. (a) A mixture of Cu and NaCl powders with a NaCl volume fraction of $V_f = 60\%$ is placed in the hole. (b) A mixture of Cu and NaCl powders with a NaCl volume fraction of $V_f = 80\%$ is placed in the hole. The mixture is (c) sintered and then (d) leached. (e) Obtained Cu foam

$V_f = 60\%$ were thoroughly mixed by pot mill [Fig. 1(a)]. Thereafter, an oxygen-free Cu plate (10 mm thickness) and an SS400 back plate (3 mm thickness) under the Cu plate were stacked and the obtained mixture was injected into a $\phi = 15$ mm hole previously drilled into the Cu plate. Namely, the SS400 plate and the bottom of the mixture were in contact during the process. Next, Cu and NaCl powders with $V_f = 80\%$ were thoroughly mixed by pot mill and injected into the hole of the Cu plate on top of the mixture of $V_f = 60\%$ [Fig. 1(b)]. Commercially available pure Cu powder (99.99% purity, average particle diameter of 1 μm) and commercially available NaCl powder (99.9% purity, sieved to a particle diameter ranging from 300 μm to 425 μm) were used. Figure 2 shows SEM images of the Cu and NaCl powder particles. The Cu powder particles were approximately spherical, while the NaCl powder particles were approximately cuboidal. The NaCl was heated in an electric furnace to remove moisture before mixing with Cu at 433 K for 30 min. Next, a cylindrical rotating tool with diameter $\phi = 25$ mm and a flat bottom was plunged into the mixture and the Cu plate [Fig. 1(c)] with the center of the hole and the center axis of the rotating tool coinciding at atmosphere. Tungsten carbide (WC) was used for the tool material, which is conventionally used in the friction stir welding of Cu (Ref 21-23). The pressing load, the rotating rate of the tool and the holding time were set to 35 kN, 1000 rpm and 60 s, respectively. Next, the sintered mixture was cut from the Cu plate by electric discharge machining then immersed in water to dissolve the NaCl [Fig. 1(d)] and obtain the FG Cu foam [Fig. 1(e)]. Cu plate only existed at the surface of the sintered mixture and it was easily removed from the sample before the dissolution process. Therefore, the composition of the mixture does not change. The weight of the mixture was measured during the dissolution process to confirm the complete removal of NaCl from the mixture. Five cylindrical FG Cu foam compression test specimens with a diameter and height of 8 mm and 7 mm, respectively, were obtained.

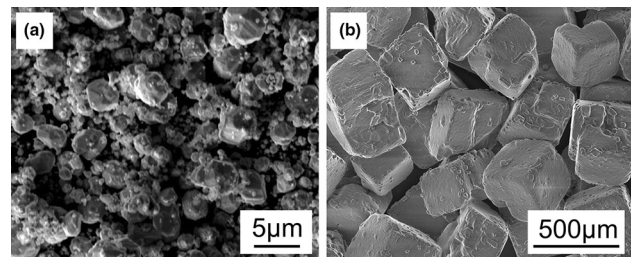


Fig. 2 SEM images of the starting materials. (a) Cu powder particles and (b) NaCl powder particles

Uniform Cu foams with $V_f = 60$ and 80% were separately fabricated by the same FPS process. Three stacked but unbonded Cu foam compression test specimens were also fabricated.

2.2 Observation of Pore Structures

To confirm that the porosities actually varied in the obtained FG Cu foams, the FG Cu foams were nondestructively observed using a cone-type microfocuss x-ray CT system. The tube voltage and tube current during the x-ray CT inspections were set at 120 kV and 30 μ A, respectively. In front of the image intensifier of the x-ray CT system, a 2-mm-thick Cu plate filter was placed. The voxel length of the three-dimensional images was 35.7 μ m. The pore structures of the obtained Cu foam at a cross section taken from the middle in the longitudinal direction were also observed by SEM.

2.3 Compression Tests

The five obtained FG Cu foams and three stacked Cu foams were subjected to compression tests. The rate of compression was set at 1 mm/min throughout the tests. The deformation behavior of the foams during the compression tests was observed by a digital video camera.

3. Experimental Results and Discussion

3.1 Pore Structures

Figure 3 shows a specimen of the obtained FG Cu foam. The upper and lower layers are the $V_f = 80$ and 60% Cu foam layers, respectively, and the samples are compressed vertically from above. The boundary between the two layers cannot be clearly observed from the surface of the specimen.

Figure 4(a) shows a center cross-sectional x-ray CT image of the obtained FG Cu foam in the longitudinal direction, which is parallel to the compression direction. The dark regions indicate pores and the bright regions surrounding the pores indicate the cell walls of the FG Cu foam. It can be seen that the upper layer ($V_f = 80\%$ layer) has more pores and higher porosity than the lower layer ($V_f = 60\%$ layer). Although the boundary between the two layers can be clearly observed, the two layers were bonded seamlessly. Figure 4(b) shows the porosity p_x distribution in the FG Cu foam in the height

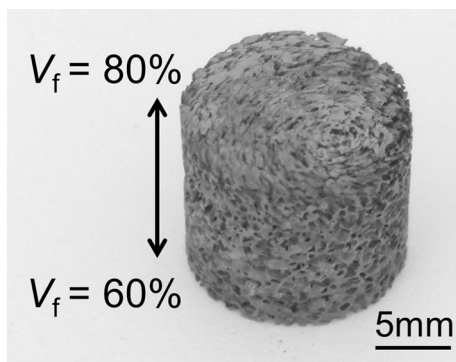


Fig. 3 Compression test specimen of fabricated FG Cu foam ($\phi = 8 \text{ mm} \times 7 \text{ mm}$). The upper and lower layers correspond to $V_f = 80$ and 60% layers, respectively

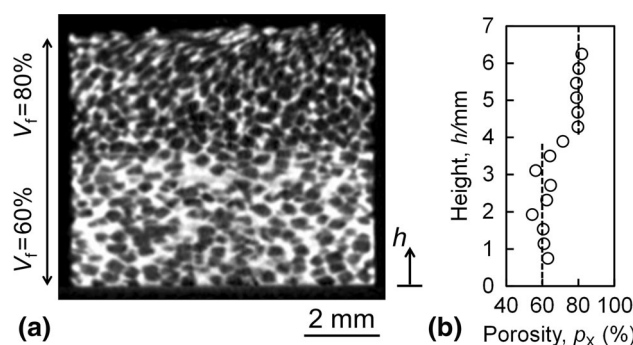


Fig. 4 (a) Cross-sectional x-ray CT image of fabricated FG Cu foam. The upper and lower layers correspond to $V_f = 80$ and 60% layers, respectively. (b) Relationship between height from bottom h of fabricated FG Cu foam and porosity p_x evaluated from x-ray CT images

direction, where the height h was measured from the bottom of the specimen [Fig. 4(a)]. p_x was evaluated as the area fraction of pores in the cross-sectional x-ray CT images taken perpendicular to the compression direction. Although there are some variations in the $V_f = 60\%$ layer, it can be seen that the porosity markedly changed at around half the height of the FG Cu foam, and both the $V_f = 80$ and 60% layers exhibited almost constant porosities. Consequently, it was found that a single FG Cu foam with changing porosities can be fabricated.

Figure 5 shows SEM images of the pore structures near the center of the $V_f = 80$ and 60% layers of the obtained FG Cu foam. A larger number of pores can be seen in the $V_f = 80\%$ layer than in the $V_f = 60\%$ layer, and their shapes are similar to the NaCl particles [Fig. 2(b)] in both layers. Although the cell walls of the pores of the $V_f = 60\%$ layer are thicker than those of the $V_f = 80\%$ layer, each pore has smaller pores on the cell walls, indicating that NaCl was removed from the pores.

3.2 Deformation Behavior

Figure 6 shows the deformation behavior of the FG Cu foam during compression tests with various strains. To clearly observe the deformation behavior, a black line was marked directly on the initial boundary of the FG Cu foams between the $V_f = 80$ and 60% layers, which was determined from the porosity distribution [Fig. 4(b)]. The dashed gray line indicates the initial boundary of the FG Cu foam at $\epsilon = 0\%$. It was found that at the beginning of the deformation of the FG Cu foam, the upper $V_f = 80\%$ layer first deformed while the lower $V_f = 60\%$ layer hardly deformed up to approximately $\epsilon = 30\%$. At this strain, the upper $V_f = 80\%$ layer was almost completely densified. Thereafter, the lower $V_f = 60\%$ layer started to deform. Namely, it was found that by controlling the distribu-

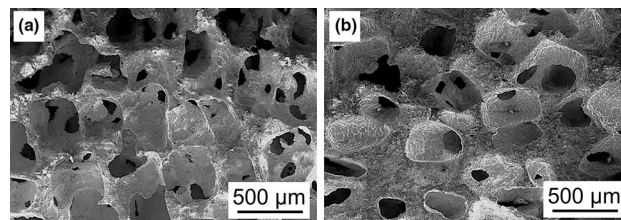


Fig. 5 SEM images of pore structures of fabricated FG Cu foam. (a) $V_f = 80\%$ layer. (b) $V_f = 60\%$ layer

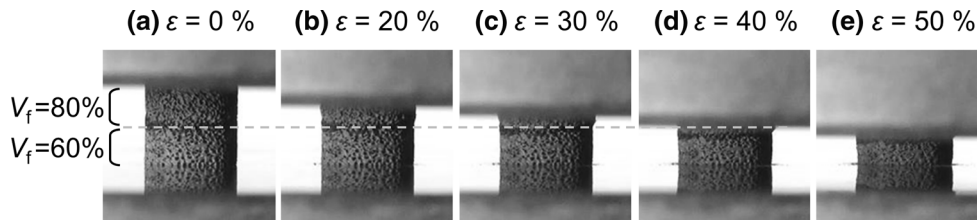


Fig. 6 Deformation images for different strains during compression tests of FG Cu foam

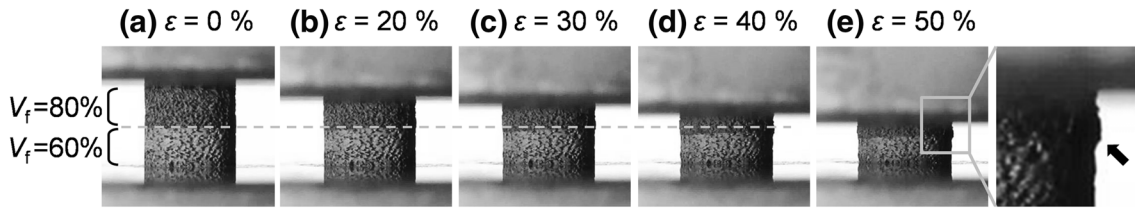


Fig. 7 Deformation images for different strains during compression tests of stacked Cu foam

tion of the porosities in the Cu foam, its deformation behavior during the compression tests can be controlled.

Figure 7 shows the deformation behavior of the stacked Cu foam during compression tests with various strains. The upper layer and lower layer correspond to the uniform Cu foam layers with $V_f = 80$ and 60% , respectively, which were not bonded. The dashed gray line indicates the initial boundary. The stacked Cu foam exhibited almost the same deformation behavior as the FG Cu foam, i.e., the deformation first began from the Cu foam layer with $V_f = 80\%$ and then from the Cu foam layer with $V_f = 60\%$. However, as shown by the arrow in Fig. 7(e), part of the densified $V_f = 80\%$ layer was extruded at the boundary, which was not observed in the deformation behavior of the FG Cu foam shown in Fig. 6. This extrusion is considered to be due to the lack of bonding and the discontinuity between the pores at the boundary layer.

3.3 Compression Stress–Strain Relation

Figure 8 shows a typical stress–strain curve obtained from the compression tests of the FG Cu foam. The compression stress–strain curves for uniform Cu foams with $V_f = 60$ and 80% (Ref 17) are also shown. The strain of the uniform Cu foams was modified to directly compare the stress–strain curves between the FG Cu foam and the uniform Cu foams in accordance with a previous study (Ref 6). By assuming that the

$V_f = 80\%$ layer only deformed at a low strain, the strain of the uniform Cu foam with $V_f = 80\%$, $\epsilon^{V_f=80\%}$, was modified to

$$\epsilon_{\text{modified}}^{V_f=80\%} = \epsilon^{V_f=80\%} \times \frac{h_1}{h_0}, \quad (\text{Eq 1})$$

where h_0 and h_1 are the heights of the entire FG Cu foam and the $V_f = 80\%$ layer in the FG Cu foam, respectively. Similarly, by assuming that the $V_f = 60\%$ layer only deformed at a high strain, the strain of the uniform Cu foam with $V_f = 60\%$, $\epsilon^{V_f=60\%}$, was modified to

$$\epsilon_{\text{modified}}^{V_f=60\%} = \epsilon^{V_f=60\%} \times \frac{h_2}{h_0} + 0.3, \quad (\text{Eq 2})$$

where h_2 is the height of the $V_f = 60\%$ layer in the FG Cu foam. h_1 and h_2 in Eq 1 and 2 were obtained from the porosity distribution shown in Fig. 4(b). In addition, because the deformation of the $V_f = 60\%$ layer (below the gray dashed line) started at approximately $\epsilon = 30\%$, as shown in Fig. 6, $\epsilon_{\text{modified}}^{V_f=60\%}$ in Eq 2 was offset by 30% strain. The FG Cu foam exhibited two plateau regions. The first plateau region appeared with a low plateau stress at the beginning of the compression tests up to approximately $\epsilon = 20\%$, which is similar to the plateau stress of the uniform Cu foam with $V_f = 80\%$. The second plateau region with a higher plateau stress subsequently appeared up to approximately $\epsilon = 50\%$. This plateau stress was similar to that obtained from the uniform Cu foam with $V_f = 60\%$. The appearance of two separate plateau regions with low and high plateau stresses during the compression tests of the FG Cu foam corresponds to the deformation behavior of the FG Cu foam. However, the deformation behavior and the corresponding stress–strain curves of FG Cu foam were more complicated than suggested by the assumptions in Eq 1 and 2, because the $V_f = 60\%$ layer of the FG Cu foam actually exhibited elastic deformation during the first plateau region and the $V_f = 80\%$ layer of the FG Cu foam continued to densify during the second plateau region. Further investigations are necessary to clarify the compression responses of FG Cu foam.

Figure 8 also shows a typical compression stress–strain curve of the stacked Cu foam, which is similar to that of the FG

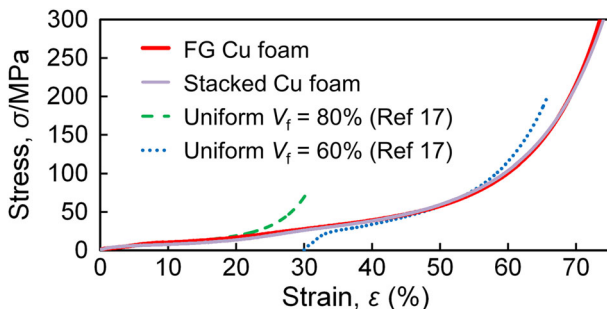


Fig. 8 Stress–strain curves of FG Cu foam and stacked Cu foam along with those of uniform Cu foams with $V_f = 80$ and 60%

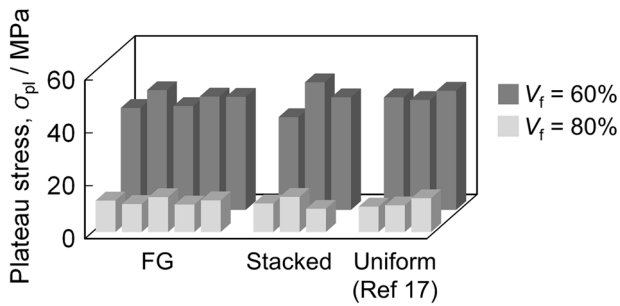


Fig. 9 Plateau stresses of first and second plateau regions of five FG Cu foams and those of three stacked Cu foams and three uniform Cu foams

Cu foam but with a slightly larger dispersion as described below.

3.4 Plateau Stresses of FG and Stacked Cu Foams

Figure 9 shows the plateau stresses of the first plateau region corresponding to the $V_f = 80\%$ layer and those of the second plateau region corresponding to the $V_f = 60\%$ layer for the five FG Cu foams, in addition to the plateau stresses of the three uniform Cu foams with $V_f = 80$ and 60% (Ref 17). The plateau stress was the average stress at a strain of 20-30% for a uniform Cu foam (Ref 24). To compare the plateau stresses between the FG Cu foams and the uniform Cu foams, Eq 1 and 2 were used to define the plateau stresses of the FG Cu foams in accordance with a previous study (Ref 10). The average stress at a modified strain of $\varepsilon_{\text{modified}}^{V_f=80\%}$, corresponding to $\varepsilon^{V_f=80\%} = 20\text{-}30\%$ using Eq 1, was defined as the first plateau stress, and the average stress at a modified strain of $\varepsilon_{\text{modified}}^{V_f=60\%}$, corresponding to $\varepsilon^{V_f=60\%} = 20\text{-}30\%$ using Eq 2, was defined as the second plateau stresses. It was found that the first and second plateau stresses obtained from the FG Cu foams were similar to those of the uniform Cu foams with $V_f = 80\%$ and $V_f = 60\%$, respectively. Therefore, it is expected that a single FG Cu foam consisting of layers with different porosities will exhibit the compression properties of uniform Cu foams with corresponding porosities during the deformation of each layer, which is consistent with the results for the FG Al foams fabricated by foaming the precursor (Ref 6, 7). Figure 9 also shows the first and second plateau stresses exhibited at each plateau region of the three stacked Cu foam specimens. These plateau stresses were defined in the same way as for the FG Cu foams described above. It was shown that the FG and stacked Cu foams exhibited almost the same tendency for each plateau stress. However, there was some dispersion in the plateau stresses for the stacked Cu foams compared with the FG Cu foams and uniform Cu foams. This dispersion is considered to be due to the lack of bonding and the discontinuity between the pores at the boundary of the stacked Cu foam.

4. Conclusion

In this contribution, bilayer FG Cu foams with $V_f = 60$ and 80% were fabricated by a friction powder sintering (FPS) process based on the sintering and dissolution process (SDP). X-ray CT observations revealed that the porosities markedly

changed around the boundary between the $V_f = 80\%$ and $V_f = 60\%$ layers of the FG Cu foam, and the two layers exhibited porosities with almost constant values and seamless bonding between the layers. From compression tests on the fabricated FG Cu foam, it was found that the $V_f = 80\%$ layer first deformed while the $V_f = 60\%$ layer hardly deformed at the beginning of the compression. Thereafter, the $V_f = 60\%$ layer started to deform. Namely, it was found that by controlling the distribution of the volume fraction of NaCl in the Cu foam, the deformation behavior of the Cu foam during the compression tests can be controlled. From the compression stress–strain curves, the FG Cu foams exhibited two plateau regions with low and high plateau stresses corresponding to the deformation behavior. The first plateau stress (low plateau stress) and second plateau stress (high plateau stress) obtained from the FG Cu foams exhibited similar values to those obtained from uniform Cu foams with $V_f = 80\%$ and $V_f = 60\%$, respectively. The stacked Cu foams exhibited almost the same deformation behavior and compression properties except for slightly larger dispersion than that in the FG Cu foams, which is considered to be due to the lack of bonding and the discontinuity between the pores at the boundary between the $V_f = 80\%$ and $V_f = 60\%$ layers.

Acknowledgments

This work was partly performed under the Cooperative Research Program of Institute for Joining and Welding Research Institute, Osaka University. The authors thank Professor T. Komoto and Professor H. Kumehara, Monodukuri Research Organization (MRO), for their helpful advices on conducting the experiments. This work was partly financially supported by JSPS KAKENHI Grant-in-Aid for Scientific Research (B).

References

1. A. Pollien, Y. Conde, L. Pambaguian, and A. Mortensen, Graded Open-Cell Aluminium Foam Core Sandwich Beams, *Mater. Sci. Eng. A*, 2005, **404**, p 9–18
2. A.H. Brothers and D.C. Dunand, Mechanical Properties of a Density-Graded Replicated Aluminum Foam, *Mater. Sci. Eng. A*, 2008, **489**, p 439–443
3. A. Hassani, A. Habibolahzadeh, and H. Bafti, Production of Graded Aluminum Foams Via Powder Space Holder Technique, *Mater. Des.*, 2012, **40**, p 510–515
4. K. Shinagawa, Shape Change and Pore Distribution in Aluminum Powder Compacts by Graded Foaming, *Porous Metals and Metallic Foams*, L.P. Lefebvre, J. Banhart, and D.C. Dunand, Ed., DEStech Publications Inc, Lancaster, 2008, p 95–98
5. R. Suzuki and K. Kitazono, Effect of Graded Pore Distribution on Thermal Insulation of Metal Foam, *J. Jpn. Inst. Metals*, 2008, **72**, p 758–762
6. Y. Hangai, K. Takahashi, T. Utsunomiya, S. Kitahara, O. Kuwazuru, and N. Yoshikawa, Fabrication of Functionally Graded Aluminum Foam Using Aluminum Alloy Die Castings by Friction Stir Processing, *Mater. Sci. Eng. A*, 2012, **534**, p 716–719
7. Y. Hangai, K. Takahashi, R. Yamaguchi, T. Utsunomiya, S. Kitahara, O. Kuwazuru, and N. Yoshikawa, Nondestructive Observation of Pore Structure Deformation Behavior of Functionally Graded Aluminum Foam by X-ray Computed Tomography, *Mater. Sci. Eng. A*, 2012, **556**, p 678–684
8. Y. Hangai, H. Kamada, T. Utsunomiya, S. Kitahara, O. Kuwazuru, and N. Yoshikawa, Compression Properties of Three-layered Functionally Graded ADC12 Aluminum Foam Fabricated by Friction Stir Welding, *Mater. Trans.*, 2013, **54**, p 1268–1273

9. Y. Hangai, K. Saito, T. Utsunomiya, S. Kitahara, O. Kuwazuru, and N. Yoshikawa, Compression Properties of Al/Al-Si-Cu Alloy Functionally Graded Aluminum Foam Fabricated by Friction Stir Processing Route, *Mater. Trans.*, 2013, **54**, p 405–408
10. Y. Hangai, K. Saito, T. Utsunomiya, O. Kuwazuru, and N. Yoshikawa, Fabrication and Compression Properties of Functionally Graded Foam with Uniform Pore Structures Consisting of Dissimilar A1050 and A6061 Aluminum Alloys, *Mater. Sci. Eng. A*, 2014, **613**, p 163–170
11. S.-Y. He, Y. Zhang, G. Dai, and J.-Q. Jiang, Preparation of Density-Graded Aluminum Foam, *Mater. Sci. Eng. A*, 2014, **618**, p 496–499
12. J. Banhart, Manufacture, Characterisation and Application of Cellular Metals and Metal Foams, *Prog. Mater. Sci.*, 2001, **46**, p 559–632
13. H. Nakajima, Fabrication, Properties and Application of Porous Metals with Directional Pores, *Prog. Mater. Sci.*, 2007, **52**, p 1091–1173
14. Y.Y. Zhao and D.X. Sun, A Novel Sintering-Dissolution Process for Manufacturing Al Foams, *Scr. Mater.*, 2001, **44**, p 105–110
15. Y. Hangai, H. Yoshida, and N. Yoshikawa, Friction Powder Compaction for Fabrication of Open-Cell Aluminum Foam by the Sintering and Dissolution Process Route, *Metall. Mater. Trans. A*, 2012, **43**, p 802–805
16. Y. Hangai, H. Yoshida, O. Kuwazuru, and N. Yoshikawa, Effect of Die Material on Compressive Properties of Open-Cell Porous Aluminum Fabricated by Friction Powder Compaction Process, *Mater. Trans.*, 2013, **54**, p 1057–1059
17. Y. Hangai, K. Zushida, H. Fujii, R. Ueji, O. Kuwazuru, and N. Yoshikawa, Friction Powder Compaction Process for Fabricating Open-Celled Cu Foam by Sintering-Dissolution Process Route Using NaCl Space Holder, *Mater. Sci. Eng. A*, 2013, **585**, p 468–474
18. M. Hakamada, Y. Asao, T. Kuromura, Y. Chen, H. Kusuda, and M. Mabuchi, Density Dependence of the Compressive Properties of Porous Copper over a Wide Density Range, *Acta Mater.*, 2007, **55**, p 2291–2299
19. Q.Z. Wang, C.X. Cui, S.J. Liu, and L.C. Zhao, Open-Celled Porous Cu Prepared by Replication of NaCl Space-Holders, *Mater. Sci. Eng. A*, 2010, **527**, p 1275–1278
20. Q.Z. Wang, D.M. Lu, C.X. Cui, and L.M. Liang, Compressive Behaviors and Energy-Absorption Properties of an Open-Celled Porous Cu Fabricated by Replication of NaCl Space-Holders, *J. Mater. Process. Technol.*, 2011, **211**, p 363–367
21. R.S. Mishra and Z.Y. Ma, Friction Stir Welding and Processing, *Mater. Sci. Eng. R-Rep.*, 2005, **50**, p 1–78
22. R.S. Mishra and M.W. Mahoney, *Friction Stir Welding and Processing*, ASM International, Materials Park, Ohio, 2007, p 155–174
23. Y.F. Sun and H. Fujii, The Effect of SiC Particles on the Microstructure and Mechanical Properties of Friction Stir Welded Pure Copper Joints, *Mater. Sci. Eng. A*, 2011, **528**, p 5470–5475
24. JIS-H-7902, Method for Compressive Test of Porous Metals, Japanese Standards Association, 2008